

Amplification of coastal-trapped waves resonantly generated by wind around Sado Island, Japan

Yosuke Igeta · Keiichi Yamazaki · Tatsuro Watanabe

Received: 22 April 2014 / Revised: 9 November 2014 / Accepted: 13 November 2014 / Published online: 26 November 2014
© The Oceanographic Society of Japan and Springer Japan 2014

Abstract Current observations were made from 4 July 2009 to 6 March 2011 with an acoustic Doppler current profiler mounted on the seafloor near the northern tip of Sado Island, Japan, and an electromagnetic current meter off the western coast of the island to investigate wind-induced coastal-trapped waves (CTW). Oscillating along-shore flows with a period of about 2 days occurred intermittently in association with atmospheric disturbances throughout the observation period. The period of the current fluctuation changed from 48 to 60 h in both summer and winter, and the fluctuations were coherent with northward wind velocity fluctuations with a period of about 2 days around the island, even though northward wind fluctuations with periods of about 3, 4, and 6 days were predominant. Thus, the 2-day-period current fluctuations were selectively enhanced by the wind. Because the wavelength of internal Kelvin waves with a 2-day period was comparable to the distance around Sado Island (210 km), we inferred that the wind-induced CTWs around the island were resonant with the 2-day-period northward wind fluctuations. This inference was supported by the results of a numerical experiment performed with a two-layer model using realistic topography, which showed that resonance effectively occurred along the western coast of the island, where the water is deep and the continental shelf is narrow,

and the resonance period was controlled by the ocean stratification strength and the shape of the island.

Keywords Wind-induced coastal-trapped wave · Resonance · Sado island · Mooring observation · Numerical experiment

1 Introduction

Upwelling and downwelling regions are generated in the upper layers of coastal oceans by winds associated with passing atmospheric disturbances that blow parallel to the coastline (e.g., Yoshida 1955). In the Northern Hemisphere, when such coastal disturbances propagate along coasts with the coast on the right, they display the characteristics of coastal-trapped waves (CTW), which fluctuate with a subinertial period (e.g., Gill and Shumann 1974). When stratification effects are predominant over the effect of the continental shelf width, the CTWs have the properties of internal Kelvin waves (IKW), whereas the CTWs have the characteristics of continental shelf waves in the opposite case (e.g., Kajiura 1974). These characteristics have been investigated analytically and numerically by assuming a coast of infinite length.

CTWs have also been analyzed around islands with coastlines of finite length. Such CTWs are called island-trapped waves (ITW) (Longuet-Higgins 1969; Hogg 1980; Brink 1999). ITWs characteristically have their wavenumbers restricted by the azimuthal length of the island. The basic characteristics of ITWs, however, are the same as those of CTWs, especially when the waves' offshore scale is small relative to the island's radius (Brink 1999).

The occurrence of ITWs has been confirmed by observations and numerical experiments: for example, sea-level

Y. Igeta (✉) · K. Yamazaki · T. Watanabe
Japan Sea National Fisheries Research Institute, Fisheries
Research Agency, 1-5939-22 Suido-cho, Chuo-ku, Niigata-city,
Niigata 951-8121, Japan
e-mail: igeta@affrc.go.jp

K. Yamazaki
Graduate School of Tokyo University of Marine Science
and Technology, 4-5-7 Konan, Minato-ku, Tokyo 108-8477,
Japan

and current fluctuations with a period of 50–70 h were generated around the Hawaiian Islands in association with a passing storm (Merrifield et al. 2002), and temperature and current fluctuations with a 24-h period were generated around the Lastovo Islands in the Adriatic Sea by strengthened sea breezes (Orlić et al. 2011).

Sado Island in the southeastern Japan Sea (Fig. 1) is basically elliptical in shape, with the major axis having a north–south orientation. However, because there is a small bay on the northeast side of the island and another on the southwest side, the island actually has an ‘S’ shape. The distance around the island is about 210 km. The coastal branch of the Tsushima Warm Current flows basically northeastward around the island, but the flow pattern varies seasonally (Watanabe et al. 2006; Aiki et al. 2007). The details of short-period fluctuations near Sado Island are unclear, although Igeta et al. (2009) reported that near-inertial fluctuations are generated around the northern tip of the island by scattering of near-inertial internal waves by the land mass.

Set-net fisheries operate year-round at about 20 sites near Sado Island. Strong coastal currents (greater than 0.4 m s^{-1} ; e.g., Kitade et al. 2011) associated with atmospheric disturbances frequently make it difficult to pull up the set nets, and these conditions can last as long as 1 month (interview with a fishery operator). Although the reported near-inertial coastal current (Igeta et al. 2009) is likely to contribute to the strong currents, it cannot entirely account for their long duration of 1 month. Therefore, it is possible that ITWs associated with atmospheric disturbances are responsible for the generation of these continuous, strong coastal currents.

In this study, we investigated the mechanism of the generation and amplification of subinertial current fluctuations around Sado Island by using data from mooring observations and the results of numerical experiments. We focused in particular on the generation and amplification processes of ITWs.

2 Observations and data

We used observation data obtained by a moored Workhorse Acoustic Doppler Current Profiler (ADCP, 300 kHz; Teledyne RD Instruments; accuracy, $\pm 4.2 \text{ cm s}^{-1}$) in the Japan Sea near the northern tip of Sado Island (Fig. 1, St. W) from 4 July 2009 to 6 March 2011. The ADCP was mounted on the seafloor at 83 m water depth; it was set up with a 4-m vertical bin resolution, and the sampling interval was 10 min. Data for which the percent-good criterion was less than 60 % were rejected for analysis and treated as missing values. In addition, current measurements were obtained off the western coast of the island at 30 m water

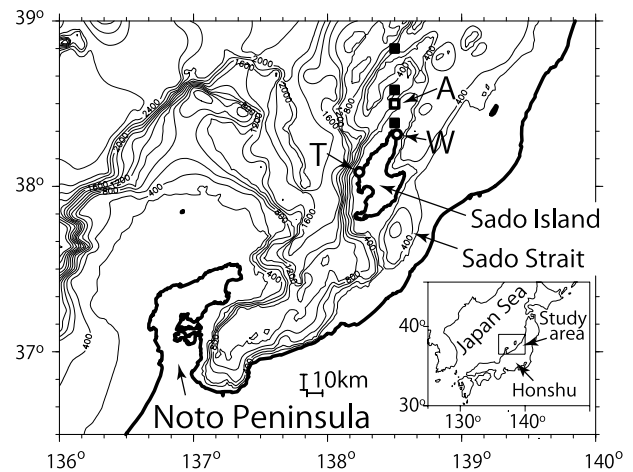


Fig. 1 Bathymetry of the seafloor around Sado Island, Japan. Numerals on the contour lines indicate water depth in meters. The inset shows the location of the study area. Open circles indicate mooring observation sites (St. W and St. T); closed squares indicate CTD stations; and the open square indicates St. A, the monitoring grid point of the GPV-MSM data set used to investigate temporal wind fluctuations

depth (Fig. 1, St. T) with an electromagnetic current meter (INFINITY-EM, JFE Advantech Co., Ltd.; accuracy, $\pm 1.0 \text{ cm s}^{-1}$) from 25 November 2009 to 5 March 2010. At both stations, missing data were estimated by linear interpolation.

For wind data, we used the Grid Point Value-Mesoscale Model (GPV-MSM) meteorological data set provided by the Japan Meteorological Agency. The grid dimensions are 0.05° latitude \times 0.0625° longitude, and the temporal resolution is 1 h. For this analysis, we extracted the northward and eastward components of wind speed from the data set at St. A (Fig. 1).

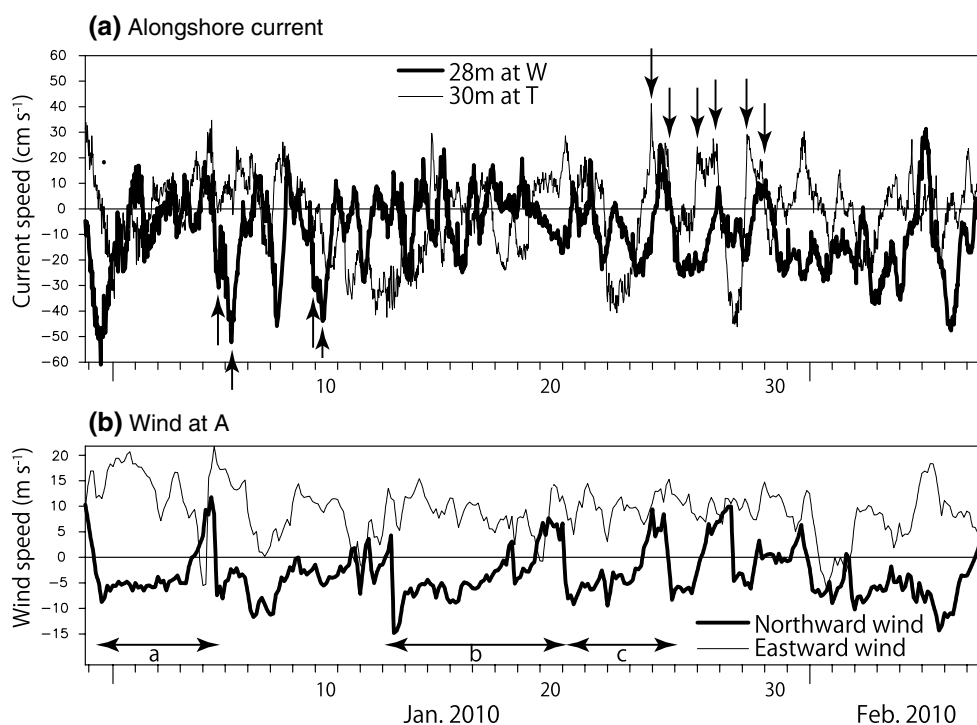
We used vertical profiles of temperature and salinity observations obtained at stations located north of Sado Island (Fig. 1) with Conductivity–Temperature–Depth (CTD) meters (SBE9/11plus; Sea-Bird Electronics, Inc.) by R/V Mizuho-maru (Japan Sea National Research Institute, Fisheries Research Agency, Japan) from July 2009 to February 2010 (which thus overlaps the period of the mooring observations). Salinity data were calibrated with an Autosol salinometer (Guildline Ltd.).

3 Observation results

3.1 Characteristics of the 2-day period current fluctuations

At Sts. W and T, the alongshore current speeds oscillated with a period of about 2 days during January and February 2010 (Fig. 2). One event started from 6 January to

Fig. 2 **a** Time series of alongshore current speeds at 28 m depth at St. W (*thick line*) and at 30 m depth at St. T (*thin line*). Positive alongshore currents are defined as currents flowing toward 202° and 22.5° clockwise at St. W and St. T, respectively (with the coast on the right). *Arrows* indicate local peaks of the alongshore current explained in Sect. 5.1. **b** Temporal variations of the northward (*thick line*) and eastward (*thin line*) wind at St. A (Fig. 1), extracted from GPV-MSM data. *Bidirectional arrows a, b, and c* indicate period explained in Sect. 5.2



around 15 January, another event started from 22 January. The fluctuations were associated with temporal fluctuations in the northward wind velocity rather than that of the eastward wind. From 22 to 30 January, the fluctuations at St. W were seen to lag those at St. T. Similar current fluctuations associated with atmospheric disturbances were observed throughout the observation period.

To investigate periodic properties of the oscillating coastal current with the 2-day period, we estimated power spectra, after dividing the current data sets of St. W into four seasonal terms: summer 2009 (09S; from 8 June to 31 October 2009); winter 2009 (09W; from 1 November 2009 to 31 March 2010); summer 2010 (10S; from 1 April to 31 October 2010); and winter 2010 (10W; from 1 November 2010 to 6 March 2011) (Fig. 3a). The spectra were calculated by a direct method with 8 degrees of freedom. Peaks occurred for periods of about 2 days (from 48 to 60 h; vertical dashed lines in Fig. 3). The peaks around the 2-day period were weak during the 10S and 10W. These peaks were not fixed at a specific period, but differed among the four seasonal terms. The energy levels of the 2-day period fluctuations (2DPF) were lower in the lower water layer (68 m depth) than in the upper layer (28 m depth) except during winter 2009. In contrast, the power spectrum estimated using the entire data set for St. T and superimposed on the winter 2009 results (09W; Fig. 3) also exhibited 2DPFs, but the signal was not as obvious as that at St. W. Scattered peaks were also found with periods from 3 to 6 days, although no

conspicuous peaks fixed at a specific period occurred at Sts. W and T. The energy levels of these peaks were comparable to those of the 2DPFs.

Power spectra of the alongshore currents were estimated using 20-day data sets to investigate growth and attenuation properties of the 2DPFs. Time variations of the power at St. T and W were obtained by doing a continuous analysis such as the running average (Fig. 4a, b). Each method is the same as that used in Fig. 3 except for three degrees of freedom. The 2DPFs were intermittently generated at St. W throughout the observation period (Fig. 4b). The 2DPFs have peaks at multiple periods from 40 to 60 h. Almost all of the 2DPFs at St. T have energetic peaks around the similar periods found at St. W when 2DPFs were observed. Events of 2DPFs were frequently found during 09S and 09W, whereas a few events were recognized during 10S and 10W. This is because of the weak peaks of the 2DPFs in the power spectra during 10S and 10W (Fig. 3a).

To quantify the phase difference between the 2DPFs between Sts. W and T, we estimated the coherence and phase difference of the alongshore currents between those at 28 m depth at St. W and those at 30 m depth at St. T, using data from 23 January 2010 to 1 February 2010 (event no. 1 shown in Fig. 4). A meaningful correlation that was larger than the 95 % confidence interval was found in the 48- to 60-h-period band, where the phase lag was 60–90° (Fig. 5a). In this analysis, this positive phase difference indicates that the 2DPFs at St. T led those at St. W.

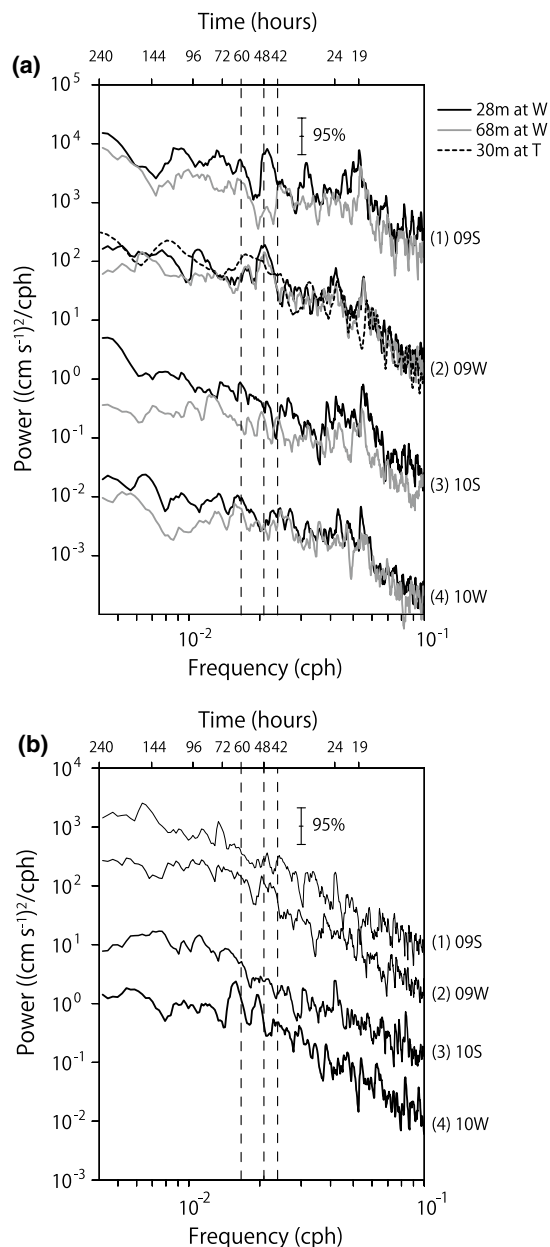


Fig. 3 **a** Power spectra of alongshore current data at 28 m depth (black lines) and 68 m depth (gray lines) at St. W, estimated during seasonal terms (1)–(4). The spectra indicated by (2)–(4) are shifted downward by 10^2 , 10^3 , and 10^4 $(\text{cm s}^{-1})^2 \text{cph}^{-1}$, respectively. Power spectra of the alongshore current data at St. T (30 m depth) are also shown, shifted downward by 10^2 $(\text{cm s}^{-1})^2 \text{cph}^{-1}$ (dotted line). **b** Power spectra of the northward wind data at St. A estimated by the same method used for the current data (see **a**)

3.2 Relation between current fluctuations and northward wind velocity

We investigated the characteristics of the northward wind blowing along the eastern and western coasts of Sado Island and the relationships between the 2DPFs and the northward wind velocity fluctuations.

The power spectra of the northward wind data at St. A, estimated by the same method used to determine the power spectra of the alongshore currents shown in Fig. 3a, showed some 2DPF peaks in the 48- to 60-h-period bands in winter 2009 and winter 2010 (Fig. 3b). However, conspicuous peaks were also found in the 3-, 4-, and 6-day-period bands, and their energy levels were larger than those of the 2DPFs, except for winter 2010.

Time variations of the power spectra of the northward wind data at St. A, estimated by the same method used in Fig. 4a and b, showed some 2DPF peaks in the 40- to 60-h-period bands during the 2DPFs found in the alongshore current at St. W (Fig. 4c). Hence, we inferred that the 2DPFs were intermittently induced by the wind. The period of northward wind is, however, not fully consistent with those of the alongshore currents.

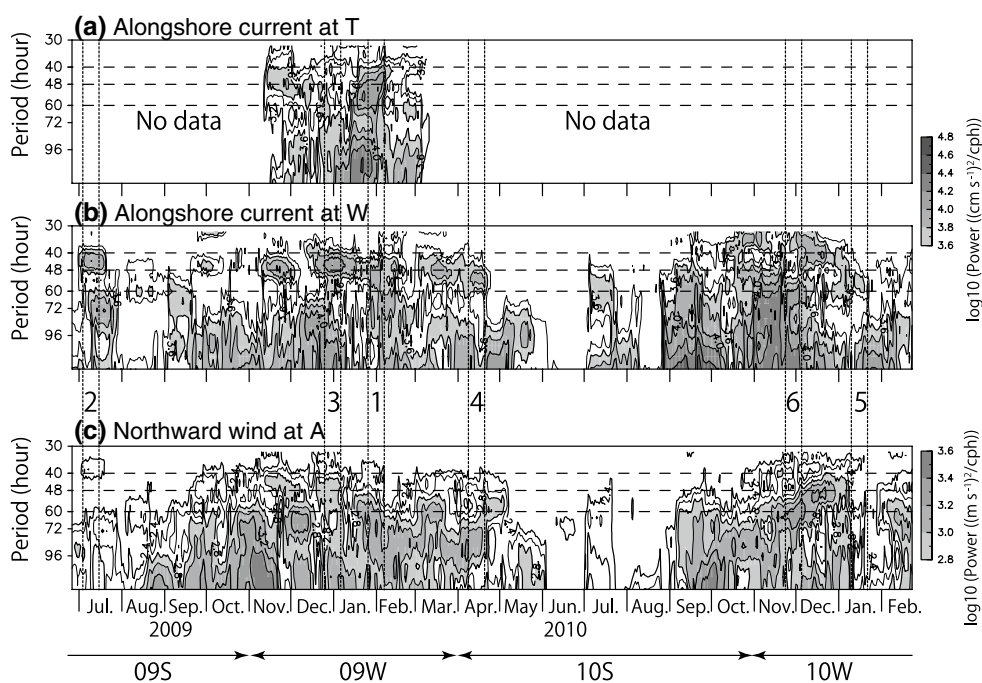
The coherence and phase differences between the northward wind at St. A and the alongshore current at 28 m depth at St. W were estimated using five data sets of 20 days including 2DPFs events shown in Fig. 4 (event nos. 1–5). Meaningful coherence can be found around the 2-day-period bands. Phase lags of the 2DPFs were generally greater than 0° (circles in Fig. 5b) where the coherence was meaningful, which indicates that the current fluctuations lagged those of the wind. The phase lags of the 2DPFs were mostly $90 \pm 50^\circ$.

3.3 Resonance of the coastal-trapped waves and the northward winds

The coherence and phase difference results for the currents and northward wind (Fig. 5a, b) strongly suggest that the 2DPFs of the currents were signals of wind-induced ITWs propagating clockwise around Sado Island. The current fluctuations were predominantly in the 40- to 60-h-period band, but the energy levels of the northward wind fluctuations with 3- and 4-day periods were higher than those of fluctuations with a period of about 2 days (Fig. 3b). We infer from these results that the 2DPFs of the currents were selectively strengthened. This suggestion is supported by the gain factors of current amplitude against the northward wind, which are obviously larger in the 42- to 60-h-period band than in the other period bands (circles in Fig. 5c). These results and those of previous studies led us to infer that the wind-induced ITWs with 2-day periods were resonant with the northward wind 2-day-period fluctuations.

Here, the alongshore current fluctuations were coherent with the eastward wind fluctuations within the 2DPFs (not shown). Gain factors and coherences, however, were not large relative to those against the northward wind (not shown). This means that the eastward wind did not directly cause the 2DPFs of current. High coherence results from high coherence between the northward wind fluctuations and the eastward wind fluctuations. Then, we investigated

Fig. 4 Time variations of the power spectra of the alongshore current at St. T (a), St. W (b), and the northward wind at St. A (c). The power spectra were estimated by using 20-day data sets and the same method used in Fig. 3 except for three degrees of freedom. Shown results were obtained by doing a continuous analysis such as the running average. Dotted lines indicate terms in which the 2DPFs events were observed. Each event is labeled by numbers sandwiched between the dotted lines. Bidirectional arrows indicate period used in Fig. 3



the northward wind only. This can be inferred from the time series of the eastward wind.

It is known that traditional CTW theory is more appropriate than ITW theory if the waves' offshore scale (width of the continental shelf or of the first baroclinic Rossby radius of deformation) is small relative to the island's radius (Brink 1999). Around Sado Island (radius about 40 km), the internal radius of deformation for the first vertical mode, estimated from the stratification obtained from the CTD data, is about 13 km ($L_{IRS} = c_s/f_{38}$) and 11 km ($L_{IRW} = c_w/f_{38}$) in summer and winter, respectively, where f_{38} is the Coriolis parameter at 38°N ($8.98 \times 10^{-5} \text{ s}^{-1}$) and c_s and c_w are the phase velocities of internal gravity waves in summer and winter, respectively. We estimated the phase velocities for a two-layer ocean model as $\sqrt{(\rho_2 - \rho_1)\rho_2^{-1} \cdot g \cdot (h_1 h_2 H^{-1})}$, where ρ_1 and ρ_2 are the densities of the upper and lower layers, respectively [$(\rho_2 - \rho_1)\rho_2^{-1}$ is 0.003 in summer and 0.0015 in winter]; H is the water depth (1,000 m); h_1 is the thickness of the upper layer (50 m in summer; 70 m in winter); and $h_2 = H - h_1$. The stratification conditions were determined by analysis of the CTD data. From the results, we judged that the offshore scale of the waves trapped around Sado Island was sufficiently small relative to the island's radius for CTW theory to be applicable.

Characteristics of CTWs are determined by the relationship between the strength of ocean stratification and the width of the continental shelf, as characterized by the stratification parameter $S = L_{IR}^2/L_S^2$ (e.g., Kajiuira 1974), where L_{IR} is the internal radius of deformation and L_S the horizontal scale of the continental shelf. If S is larger (smaller) than 1.0, the CTWs have the characteristics of

IKWs (continental shelf waves). Along the western coast of Sado Island, the continental shelf width (L_S) is about 10 km (see Fig. 1). Thus, the CTWs around Sado Island can be considered to have the characteristics of IKWs, since the parameter S is larger than 1.0 in both summer and winter. This result indicates that the ITWs with a 2-day period can be treated as IKWs around Sado Island.

To compare the wavelength of the CTWs propagating around Sado Island with the distance around the island (210 km), we estimated the dispersion curves of the IKWs for the first vertical mode under the summer and winter stratification conditions (Fig. 6, A and B, respectively). IKWs with a wavelength of 210 km have periods of about 48 and 60 h under the stratification conditions of summer and winter, respectively. These results clearly indicate that resonance can occur between CTWs with a 2-day period and the northward wind fluctuating with a period of about 2 days around Sado Island. In addition, the stratification condition may determine the resonance period.

Other waves needed to be discussed are bottom trapped shelf waves (BTSW) and higher vertical modes of the IKWs. The BTSWs can exist within the step type shelf region under the two-layer stratification condition mentioned above. This wave has small wavenumber (smaller than L_{IR}) and its motion is confined in the bottom layer (Kajiuira 1974). Higher vertical modes of the IKWs are also able to exist under continuous stratification conditions and their wavelengths are shorter than those of the first vertical mode. For both cases, several waves can exist along eastern and western coasts of the island, respectively, since, under such conditions, resonance with the northward wind cannot effectively occur.

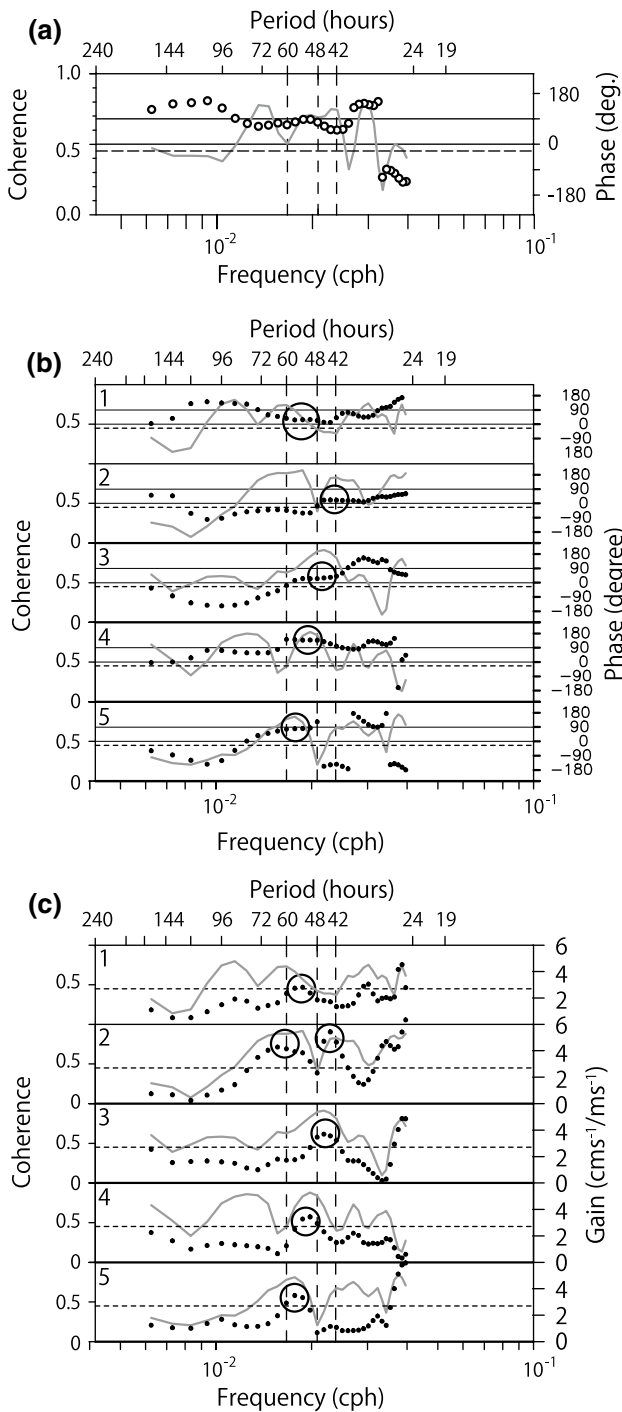


Fig. 5 **a** Coherence (gray line) and phase lags (open circles) between alongshore currents at 28 m depth at St. W and alongshore currents at 30 m depth at St. T, estimated using 20-day data for the period event named no. 1 (Fig. 4), were observed. The dashed horizontal line indicates the 95 % confidence limit. **b** Coherence (gray lines) and phase lags (black dots) between the alongshore currents at 28 m depth at St. W and the northward wind at St. A, estimated using 20-day data for each 2DPFs event term (nos. 1–5 shown in Fig. 4). The horizontal dashed lines indicate the 95 % confidence limit. **c** Gain factors (black dots) of current amplitude against the northward wind for each 2DPFs event term. Gray lines and dotted lines indicate the coherence and the 95 % confidence limit

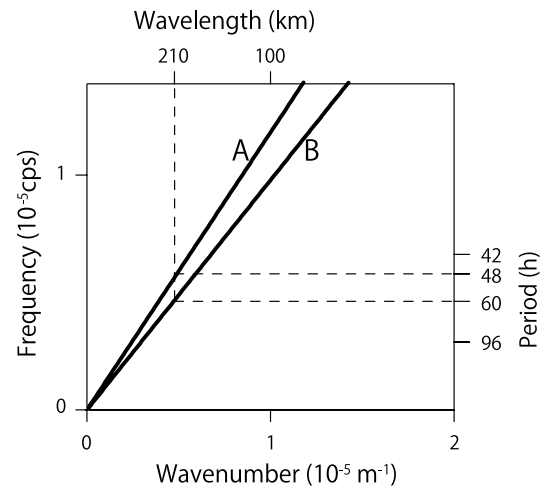


Fig. 6 Dispersion relations of the internal Kelvin waves. Curves A and B were estimated using summertime and wintertime stratification conditions, respectively

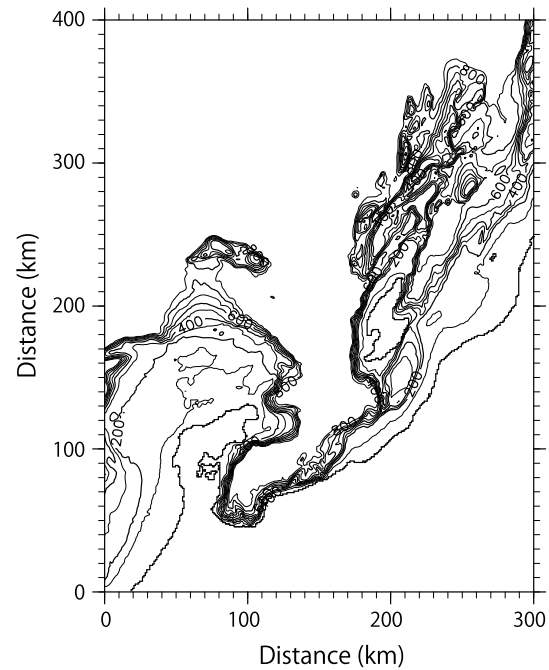


Fig. 7 Computational domain. A realistic coastline and simplified bottom topography were used in the numerical experiments. Depths greater than 1,000 m were set to 1,000 m

4 Numerical experiments

4.1 Numerical model and experiments

We investigated the detailed mechanisms of wave generation and amplification by performing numerical simulations. First, we confirmed the occurrence of resonance between the CTWs and the northward wind around Sado

Island. Then, we examined how the resonance period was determined.

We used the two-layer model described by Kitade and Matsuyama (2000). The computational domain was 400 km from north to south and 300 km from east to west (Fig. 7), and the horizontal grid size was set to 1 km \times 1 km. The topographic data were from the JTOPO30 data set, provided by the Japan Marine Information Center. For simplicity, depths deeper than 1,000 m were set to 1,000 m and depths shallower than 100 m were set to 100 m. Clamped and sponge open boundary conditions were applied to allow surface Ekman transport across open boundaries and to reduce disturbances near them. The non-slip condition was applied along rigid boundaries.

We performed two sets of experiments, a set using summertime stratification conditions (EXP-S) and another using winter conditions (EXP-W). The stratification conditions adopted were the same as those used to estimate the dispersion curves of the IKWs (see Fig. 6, Sect. 3.3). Thus, the layer interface does not come into contact with the sea bottom. Northward winds fluctuating with an amplitude of 5 m s⁻¹ and a period of about 2 days were assumed to occur uniformly over the whole model domain. In each set of experiments, the fluctuation period of the northward wind was varied from 42 to 60 h at 2-h intervals. Thus, we performed 20 experiments in total (two sets of 10 each). We named each experiment according to the stratification condition and the fluctuation period of the northward wind. For example, in experiment S-42, summertime stratification conditions were used and the northward wind fluctuated with a 42-h period.

4.2 Experimental results

Figure 8 shows the simulated temporal variation of the alongshore current obtained at the grid containing St. W in the W-56 experiment. The alongshore current fluctuates with a period of 56 h, and the fluctuation amplitudes clearly increase with time. This result indicates that the wind-induced 2DPF of the currents around Sado Island were amplified by the northward wind fluctuating with about 2-day period.

Figure 9a shows the horizontal distribution of the phase lags and amplitude of the 56-h fluctuations estimated by harmonic analysis by using interface displacement data of the W-56 results. Around Sado Island, the amplitude of the interface displacement fluctuations falls exponentially with distance from the coast, and the co-phase lines from 0° to 360° radiate out from the island. This result indicates that the CTWs move clockwise around the island every 56 h. Because the initial phase was set at 112 h in this analysis, the phase indicates the lags of the northward wind fluctuation. The 180° co-phase line extends from the southern tip

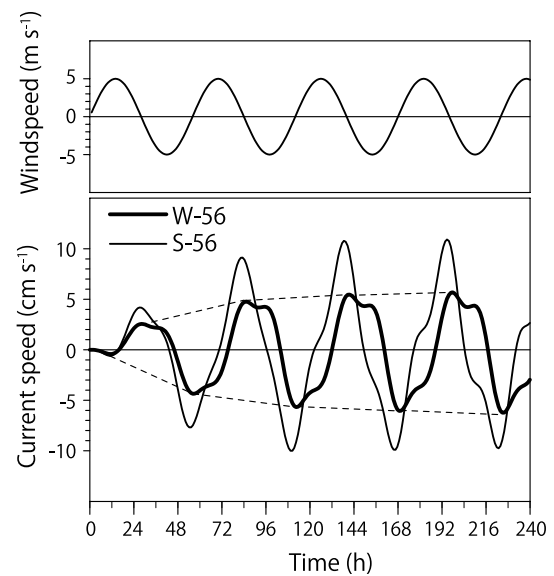


Fig. 8 Temporal variations of the currents with the coast on the right at the grid point containing St. W, obtained from numerical experiments W-56 and S-56. The top panel shows the temporal variations of the northward wind used in these experiments

of Sado Island, and the 180° to 300° phases are distributed along the western coast of the island. This distribution indicates that the upwelling (downwelling) parts of the CTWs were effectively resonant with the southward (northward) wind along the western coast of Sado Island. In addition, we can infer that effective resonance occurs along the southeastern coast of the island.

Around the eastern coast of the Noto Peninsula, similar resonance processes occur, because the distributions of the amplitude and co-phase lines are similar to those around Sado Island. The amplified CTWs move eastward along the Honshu coast but attenuate rapidly at the mouth of the Sado Strait, where the 0° to 180° phases are distributed. This suggests that the CTWs are effectively weakened by the northward (southward) wind around the mouth of the strait.

5 Discussion

5.1 Basic resonance process

The period causing resonance changed from 48 to 60 h every 2DPFs events, as shown in Fig. 5. Here, we discuss the mechanism of these resonance periods. We examined the gain factors of the alongshore currents at St. W against the wind speeds (Fig. 10) estimated by using the maximum current and wind amplitudes obtained and used in each experiment. The maximum value was extracted from the current data obtained from the third oscillation of each experiment. We judged the maximum current amplitude

Fig. 9 **a** Horizontal distributions of the phase lag (*solid lines*) and the amplitude of the interface displacement (*dashed lines* and *shading*) estimated using the results of W-56 (winter stratification condition and northward wind fluctuating with a 56-h period). *Numerals* beside the *solid lines* indicate degrees. The contour interval for phase lag is 20° and that for amplitude is 50 cm. **b** The same as **(a)**, but showing the results of S-56 (summer stratification condition and northward wind fluctuating with a 56-h period)

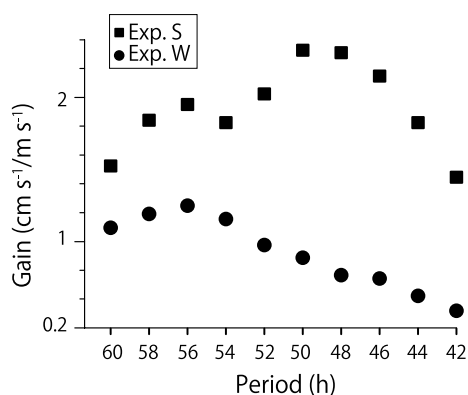
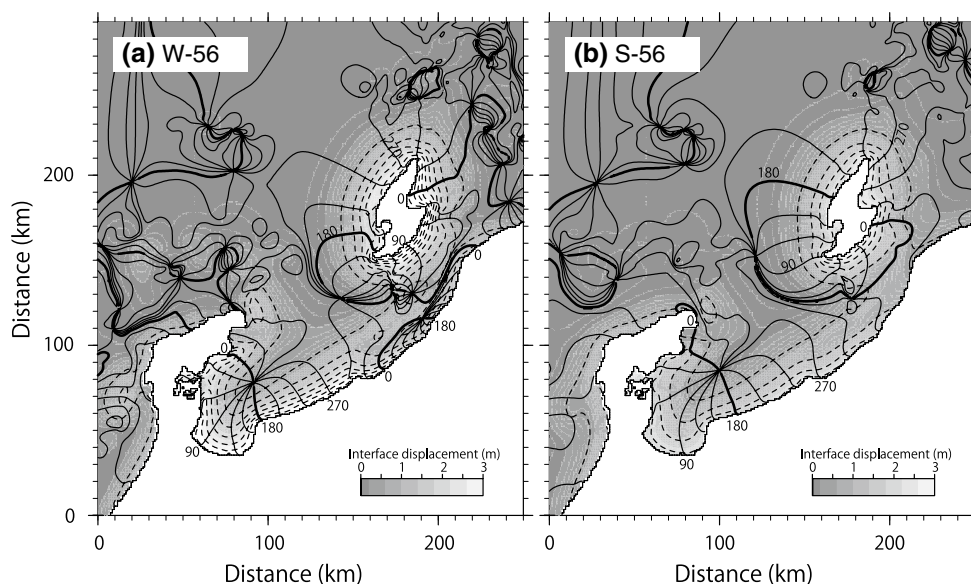


Fig. 10 Gain factors of current amplitude at St. W against the northward wind obtained from all numerical experiments. *Squares* and *circles* indicate the results of exp. S (using summertime stratification) and exp. W (using wintertime stratification), respectively

to become larger as the fluctuation period approached its resonance period. The resonance periods were around 48 h under strong (EXP-S) and 56 h under weak (EXP-W) stratification conditions. The amplitude and phase distribution of the 48-h period fluctuation obtained in S-48 (not shown) were quite similar to those in Fig. 9a, which indicates that the 48-h and 56-h period CTWs are effectively resonant with wind fluctuations around the western and southeastern coasts. Therefore, the resonance period reflects the strength of the stratification.

In addition, a secondary peak was found at around 56 h under strong stratification (EXP-S). The existence of this peak suggests that another factor exists that determines the resonance period. Figure 9b shows the horizontal distribution of the phase lags of the 56-h fluctuations due to interface displacement in S-56. The distributions of the

amplitude and phase are similar to those in W-56 (Fig. 9a), except for around the western coast of Sado Island. The 180° co-phase line extends offshore from the middle part of the western coast of the island, which indicates that effective resonance occurs around the northwestern and southeastern coasts of the island.

The resonance pattern shown in Fig. 9b induces attenuation and amplification of the 'head part' ($270-0^\circ$ in Fig. 9b) and 'tail part' ($180-270^\circ$ in Fig. 9b) of a crest of the CTW, respectively. The mechanism works at the trough of the CTW as well. This causes distortion in the height of the interface of the CTW, and such distortions can be found in the time variation of the current (S-56 in Fig. 8). The resonance pattern of W-56 (Fig. 9a) amplifies the whole of the CTW along the western coast of Sado island, and its shape is distorted into one reflecting the island, i.e., the CTWs have two peaks per half cycle (W-56 in Fig. 8). In other words, secondary fluctuations with periods shorter than wind forcing periods are generated by collaboration between the 'S' shape of the Sado island and wind which is spatially uniform. The periods of the secondary fluctuations are provided by horizontal scales of the coastal lines. Similar signals can be recognized in the observed current fluctuations at St. T (arrows in Fig. 2).

Nonlinearity is generally important for distortion of the waves. In this case, however, nonlinearity was judged to be weak, because the current velocities of the CTWs (up to 60 cm s^{-1}) were deemed small relative to the propagation speed of the CTWs (about 1.2 m s^{-1}) (Fig. 2). This fact supports the aforementioned distortion process. On the other hand, strong currents faster than 80 cm s^{-1} were several times observed in association with atmospheric disturbances. In these cases, nonlinearities were considered to be strong. The wave form distortions of such cases are challenges for the future.

These results indicate that the resonance periods are controlled not only by the strength of the stratification but also by the shape of the island. This mechanism is a new finding of this work. We consider the predominant period of the current fluctuation around Sado Island to be determined through this process. As a result, in the spectral analysis of the current data (Fig. 3) several peaks were obtained at around 48–60 h.

The 2DPFs in 09S and 09W shown in Fig. 3a have quite similar periods (48 h), though they should have different periods because of the different stratification. This discrepancy means that the periods of the energetic 2DPFs were not controlled completely by stratification conditions, but depended on the periods of the energetic wind. In other words, the periods of the energetic 2DPFs found in currents were considered to be determined by superposition of forced motions and free waves of the CTWs.

5.2 Resonance processes due to typical wind fluctuations

Here, we show the resonance processes generated by probable wind fluctuations using our two-layer model. Some cases were found in which the wind, after blowing southward for several days, shifted to northward, and the northward wind continued to blow for a full day (Fig. 2b, arrows a–c). These cases were associated with the passing of an anticyclone over the southern part of Sado Island during the winter monsoon. Similar wind fluctuations with opposite wind direction are associated with typhoons passing from west to east in the summer. We therefore modeled these wind fluctuations (solid line in Fig. 11a) as a southward wind persisting for 6 days, after which the wind blew northward for a day. In this numerical experiment, we obtained the current fluctuations shown in Fig. 11b (solid line), calculated at St. W. While the wind was blowing southward, the current flowed with the coast on the left. In this situation, stationary upwelling and downwelling regions are located around the northern and southern ends of the island (Fig. 12, 100 h).

This situation can be interpreted as follows: (1) an upwelling region is generated along the western coast by the southward wind (Fig. 12, 20 h); (2) the upwelling region propagates clockwise around the island with the coast on the right (Fig. 12, 20–100 h); (3) along the eastern coast the upwelling region is attenuated by the southward wind generating downwelling regions; (4) interface displacement is canceled out along the middle part of the eastern coast. The downwelling region distributed around the southern part of the island forms by the same mechanisms.

After the southward wind attenuates, the upwelling and downwelling regions start to propagate clockwise around the island as a CTW (Fig. 12, 100–140 h). The CTW is amplified around the northwestern and southeastern coasts

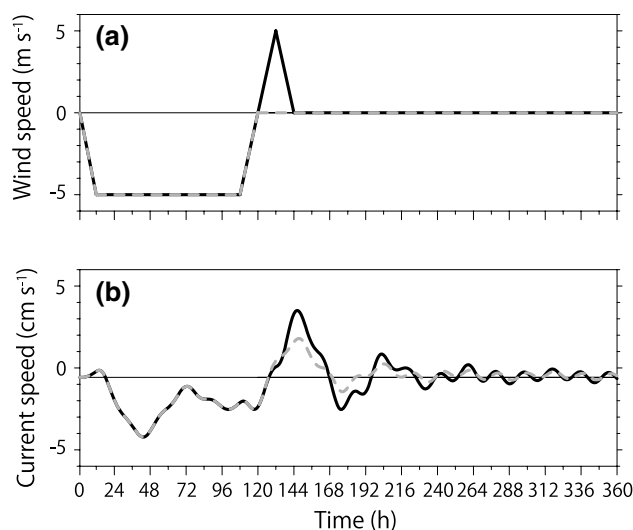
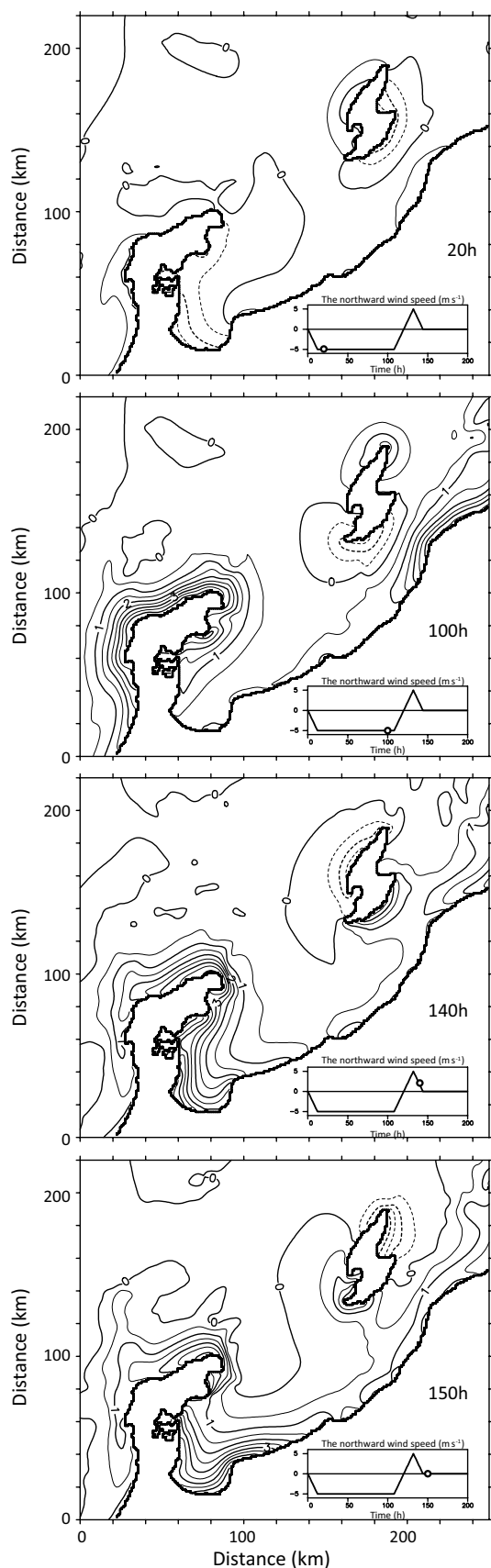


Fig. 11 a Temporal variations of the northward wind used in two experiments to investigate how typical wind fluctuations affect current. Experiment 1, *solid black line*; experiment 2, *dashed gray line*. b Temporal variation of the current with the coast on the right at the grid point containing St. W obtained from experiment 1 (*solid black line*) and experiment 2 (*dashed gray line*)

of the island by the change of the wind direction from southward to northward (Fig. 12, 140–150 h). This process is the same as the resonance processes described in Sects. 4.2 and 5.1. As a result of this process, an alongshore current with the coast on the right at St. W has an amplitude twice as large as that of the current obtained by the numerical experiment using only the southward wind (i.e., without the subsequent northward blow; Fig. 11, gray dashed lines).

6 Summary

We investigated the generation and amplification of coastal-trapped waves (CTW) around Sado Island, Japan, by using current observations at two sites, made with a current meter and a seafloor-mounted ADCP. Subinertial current fluctuations with a period of about 2 days were observed in association with wind fluctuations throughout the observation period. The 2-day-period fluctuations (2DPF) propagated with the coast on their right, and the period varied from 40 to 60 h among 2DPFs events. The 2DPFs of the current were coherent with the 2DPFs of the northward wind, but the 2DPFs of the northward wind did not show remarkable predominance compared with the 2DPFs of the current. These results suggest that the 2DPFs of the currents were selectively strengthened and that CTWs with a period of 2 days were resonantly generated by the northward wind. This inference is supported by the fact that the distance around Sado Island (210 km) agrees with the wavelength



◀ **Fig. 12** Sequential patterns of interface displacement at 20, 100, 140, and 150 h. *Solid and dotted lines* indicate upwelling and downwelling regions, respectively. The contour interval is 50 cm. Temporal variations of the northward wind used in this experiment are also shown in each panel. *Open circles* indicate the wind speed at the indicated time

of the first vertical mode internal Kelvin waves (IKW), i.e., the CTWs around Sado Island in the 48- to 60-h-period band.

We investigated the details of the resonance process between the CTWs and the northward wind by conducting numerical experiments with a two-layer ocean model with realistic topography under strong and weak stratification conditions. In the whole model domain, northward winds with 2DPFs were assumed to be distributed uniformly, and the period was varied from 42 to 60 h. The model results showed that resonance effectively occurred along the western and southeastern coasts of the island. The resonance period depended on the stratification conditions; it was 48 h under the summer stratification condition and 56 h under the winter stratification condition. These results indicate that the CTWs can be resonant with the winds around Sado Island by similar mechanisms reported by previous studies around other islands. However, under the summer stratification condition, there was not just a single resonance period but two (both 48 and 56 h), because of the amplification of the ‘tail’ part of the CTWs that resulted from effective resonances occurring around the northwestern and southeastern coast of the island. As a result, we conclude that the resonance period is controlled not only by the strength of the stratification but also by the shape of Sado Island.

Here, some outstanding issues remain. One of the issues is included in the interrelation between 2DPFs at St. W and those at St. T. During event no. 3 (Fig. 4), 40- to 48-h-period fluctuations were weak at St. T whereas they were strong at St. W. The other issue concerns event no. 6 in Fig. 4; although predominance of about 60-h-period fluctuations can be found in current and wind, estimated gain factors were not large relative to the other events shown in Fig. 5c. The latter results in the weak peaks of currents in the 2DPFs in winter 2010 (Fig. 3a) in spite of the energetic peaks of wind in the 2DPFs (Fig. 3b). To clarify these issues, multiple problems should be investigated, e.g., the relation between local topographies around mooring stations (such as reefs and curvature of coastal lines) and non-linearity due to strengthening of the current, separation of forced motion due to wind (coastal jets) from resonance signals of CTWs, resonance processes by wind rotation. These are challenges for the future.

Acknowledgments We thank Dr. Y. Kitade, Dr. T. Senjyu, Dr. H. Nakamura, and Dr. N. Hirose for useful discussions. This research was supported by the Research Project for Utilizing Advanced Technologies in Agriculture, Forestry, and Fisheries in Japan. GPV-MSM data were provided by the Japan Meteorological Agency. The figures were produced by the GFD-DENNOU software library.

References

- Aiki T, Isoda Y, Yabe I, Kuroda H (2007) Seasonal variations of surface flow around Toyama Bay. *Oceanogr Japan* 16:291–304 (in Japanese with English abstract)
- Brink KH (1999) Island-trapped waves, with application to observations off Bermuda. *Dyn Atmos Oceans* 29:93–118. doi:[10.1016/S0377-0265\(99\)00003-2](https://doi.org/10.1016/S0377-0265(99)00003-2)
- Gill AE, Shumann EH (1974) The generation of long shelf waves by the wind. *J Phys Oceanogr* 4:83–90
- Hogg NG (1980) Observations of internal Kelvin waves trapped round Bermuda. *J Phys Oceanogr* 10(1353–1376):1980. doi:[10.1175/1520-0485010<1353:OOIKWT>2.0.CO;2](https://doi.org/10.1175/1520-0485010<1353:OOIKWT>2.0.CO;2)
- Igeta Y, Kumaki Y, Kitade Y, Senjyu T, Yamada H, Watanabe T, Katoh O, Matsuyama M (2009) Scattering of near-inertial internal waves along the Japanese coast of the Japan Sea. *J Geophys Res* 114:C10002. doi:[10.1029/2009JC005305](https://doi.org/10.1029/2009JC005305)
- Kajiura K (1974) Effect of stratification on long period trapped waves on the shelf. *J Oceanogr Soc Japan* 30:271–281
- Kitade Y, Matsuyama M (2000) Coastal-trapped waves with several-day period caused by wind along the southeast coast of Honsyu, Japan. *J Oceanogr* 56:727–744
- Kitade Y, Igeta Y, Fujii R, Ishii M (2011) Amplification of semidiurnal internal tide observed in the outer part of Tokyo Bay. *J Oceanogr* 67:613–625. doi:[10.1007/s10872-011-0061-0](https://doi.org/10.1007/s10872-011-0061-0)
- Longuet-Higgins MS (1969) On the trapping of long-period waves round islands. *J Fluid Mech* 37:773–784. doi:[10.1017/S0022112069000875](https://doi.org/10.1017/S0022112069000875)
- Merrifield MA, Yang L, Luther DS (2002) Numerical simulations of a storm-generated island-trapped wave event at the Hawaiian Islands. *J Geophys Res* 107(C10):3169. doi:[10.1029/2001JC001134](https://doi.org/10.1029/2001JC001134)
- Orlić M, Paklar GB, Dadić V, Leder N, Mihanović H, Pasaric M, Pasaric Z (2011) Diurnal upwelling resonantly driven by sea breezes around an Adriatic island. *J Geophys Res* 116:C09025. doi:[10.1029/2011JC006955](https://doi.org/10.1029/2011JC006955)
- Watanabe T, Katoh O, Yamada H (2006) Structure of the Tsushima Warm Current in the northeastern Japan Sea. *J Oceanogr* 62:527–538. doi:[10.1007/s10872-006-0073-3](https://doi.org/10.1007/s10872-006-0073-3)
- Yoshida K (1955) Coastal upwelling off the California coast. *Rec Oceanogr Works Jpn* 2(2):1–13